Mechanical and friction properties of thermoplastic polyurethanes determined by scanning force microscopy

Bénédicte Mailhot-Jensen, K. Komvopoulos, B. Ward, Y. Tian, G. Somorjai

Mechanical and friction properties of thermoplastic polyurethanes determined by scanning force microscopy

B. Mailhot[a)]
Department of Chemistry, University of California, Berkeley, California 94720
and Lawrence Berkeley National Laboratory, Material Science Division, Berkeley, California 94720

K. Komvopoulos[b)]
Department of Mechanical Engineering, University of California, Berkeley, California 94720

B. Ward and Y. Tian
Polymer Technology Group, Inc., Berkeley, California 94710

G. A. Somorjai
Department of Chemistry, University of California, Berkeley, California 94720
and Lawrence Berkeley National Laboratory, Material Science Division, Berkeley, California 94720

Abstract

The mechanical and friction properties of additive-free polyurethane (PUR) consisting of polyether soft segments of polytetramethyleneoxide and hard segments (HS) comprising 4,4'-diphenylmethane diisocyanate and 1,4-butanediol as a chain extender were studied by scanning force microscopy. The hardness and elastic modulus of PUR containing 42, 57, 69, and 100 wt % HS were determined from nanoindentation experiments performed with a diamond tip of nominal radius of curvature equal to ~20 μm and maximum indentation load in the range of 10–500 μN. The mechanical properties of PUR were found to strongly depend on the HS content and contact load. The elastic modulus of PUR with 42 wt % HS was found to decrease with increasing load due to the high softness of this material that influenced the measurements. The friction characteristics of the samples with 42, 57, and 69 wt % HS were studied in order to evaluate the dependence of the coefficient of friction on load and sliding speed. The PUR with 57 wt % HS exhibited the lowest coefficient of friction. Depending on the PUR composition, remarkably different friction behaviors were obtained. The observed mechanical behavior and friction characteristics are interpreted in terms of the chemical composition and microstructure of the samples.

I. INTRODUCTION

Segmented polyurethane (PUR) elastomers exhibit excellent mechanical properties and good blood and tissue compatibility. Therefore, these materials are ideal for the fabrication of medical devices, such as cardiac pacemakers, prostheses, catheters, and heart-assist devices. PUR elastomers are also frequently used in many other nonmedical applications including adhesives, sporting equipment, artificial leather, and cable insulation. Although the bulk properties of PUR have been widely studied,[1–14] the surface properties, such as hardness, elastic modulus, and friction, which are of great importance in all the earlier-mentioned applications, have received relatively less attention. Since in many situations polymers are subjected to compressive (and shear) surface traction, characterization of the surface mechanical properties under the presence of a compressive load is more appropriate than bulk measurements obtained from simple stretching experiments. Unfortunately, basic knowledge of the surface mechanical properties of polyurethanes is relatively sparse.

Polyurethane can be considered as a copolymer comprising two incompatible segments. The glass transition temperature of one of the segments is well below the ambient (~−40 °C) and is therefore considered to be a rubbery or ''soft'' segment (SS), whereas the glass transition temperature of the other segment is well above the ambient (~50 °C) and is therefore considered to be a rigid or ''hard'' segment (HS).[3] By varying the proportion of hard and soft segments, a wide range of mechanical properties can be obtained.[4]

The urethane groups of the HS form hydrogen bonds mainly by the interaction of the NH groups with the urethane carbonyl function and, to a lesser extent, with the ether groups[4] (Fig. 1). In the solid state at room temperature, most of the NH groups are hydrogen bonded to either the HS (C=O groups) or the SS (–O– groups).[5] The C=O urethane groups form hydrogen bonds only with the HS (NH groups). As a consequence, the rigid and polar HS segments interact strongly with each other (through hydrogen bonding) and do not mix homogeneously at ambient conditions with the flexible and less polar segments.[3] PUR is known to undergo a microphase separation leading to the formation of small

crystalline HS domains.[1,6–13] Microphase separation increases with the HS content,[6] and can be estimated from the infrared spectrum.[13] The carbonyl vibration region gives information about interurethane hydrogen bonding (Fig. 2). When the urethane group is hydrogen bonded, the wavenumber of bonded carbonyl vibration (~1700 cm^{-1}) shifts to a higher value than that corresponding to the nonbonded carbonyl vibration (~1730 cm^{-1}).[13] Figure 2 shows that both hydrogen-bonded and nonhydrogen-bonded C=O groups are present in all the samples, and that the intensity ratio of hydrogen-bonded to nonbonded C=O vibration bands increases with the HS content. This trend indicates that the degree of microphase separation increases with the HS content. Each composition contains nonbonded HS and hydrogen-bonded HS. The nonbonded HS are randomly distributed in the material while the hydrogen-bonded HS are associated with each other within small crystalline domains (Fig. 3). The concentration of crystalline domains increases with the HS content. There are two phases in the polymer: (a) a crystalline phase consisting of hydrogen-bonded (associated) HS and (b) an amorphous phase consisting of SS and nonassociated HS. Increasing the HS content (i.e., promoting microphase separation) enhances the mechanical properties of segmented PUR.[14]

The review of the literature indicates that despite significant applications and increasing demands for polymer structural materials, fundamental knowledge of the surface properties of elastomers and basic understanding of the underlying friction and deformation mechanisms is rather limited. Consequently, the principal objective of this study was to examine the surface mechanical properties and friction characteristics of different PUR compositions using state-of-the-art surface force microscopy. The dependence of hardness and elastic modulus on the HS content and microphase separation, and the effects of microstructure, contact load, and sliding speed on the friction behavior are interpreted in light of nanoindentation and friction results. In addition, the dominant friction mechanisms are discussed in terms of the material composition and associated deformation behavior.

II. EXPERIMENTAL PROCEDURES

A. Sample preparation

Additive-free PUR samples (Polymer Technology Group, Inc.) comprising polyether SS consisting of polytetramethylene oxide (PTMO), with a molecular weight of 1000 g/mol, and HS produced from 4,4′-diphenylmethane diisocyanate (MDI) and 1,4-butanediol (BDO) as a chain extender were used in this study. Four polymers consisting of PTMO/MDI/BDO containing about 42, 57, 69, and 100 wt % HS were prepared. The glass transition temperature T_g, measured by the manufacturer using differential scanning calorimetry, and molecular weight of each sample are given in Table I. The variation of the bulk mechanical properties, such as tensile strength, ultimate elongation, elastic modulus, and hardness, measured according to the American Society for Testing and Materials standards are listed in Table II.

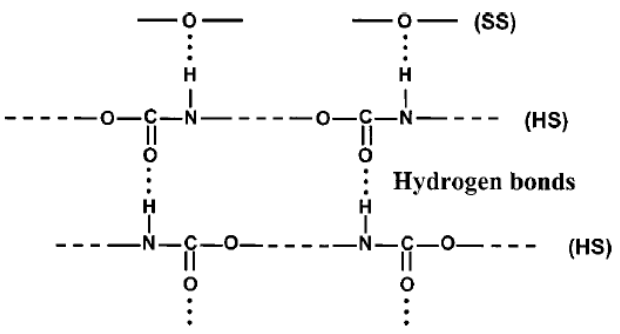

FIG. 1. Hydrogen bonding between segments in urethane groups.

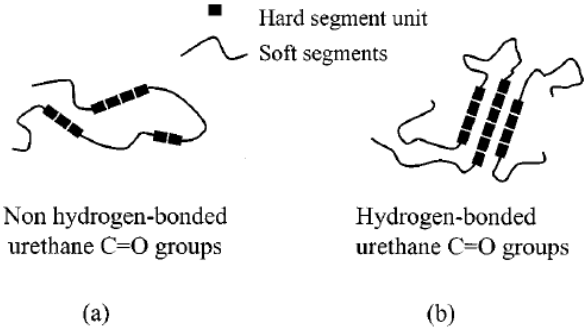

FIG. 3. Schematic representation of microphase separation in PUR: (a) nonhydrogen-bonded HS, and (b) hydrogen-bonded HS with formation of crystalline microdomains.

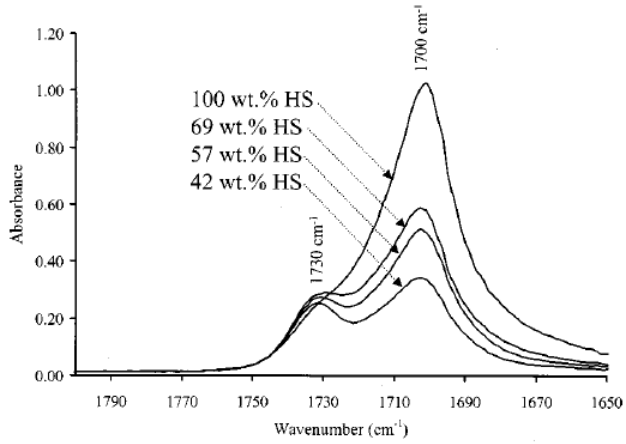

FIG. 2. Infrared spectra of PUR containing 42, 57, 69, and 100 wt % HS (1730 cm^{-1}: free C=O stretching; 1700 cm^{-1}: H-bonded C=O stretching).

TABLE I. Molecular weight and glass transition temperature of polyurethane specimens.

HS (wt %)	Molecular weight[a] (g/mol) $\overline{M_n}=\frac{\Sigma N_i M_i}{\Sigma N_i}$	$\overline{M_W}=\frac{\Sigma N_i M_i^2}{\Sigma N_i M_i}$	T_g (°C) SS	HS
42	133213±4595	245708±5261	−49±0	43±3
57	74315±3387	109698±4911	−37±13	58±11
69	76557±558	108508±866	NA[b]	42±4

[a]Space i comprises N_i macromolecules of M_i molecular weight.
[b]The T_g for the 69 wt % HS content could not be measured accurately (signal too low).

TABLE II. Typical bulk mechanical properties of polyurethane specimens.

HS (wt %)	Tensile strength (MPa)	Ultimate elongation (%)	Elastic modulus (MPa)	Hardness[a] (Shore)
42	31±4	594±54	21±1	80±2.6 A (~3.75)
57	48±4	461±48	101±21	54±0.5 D (~4.50)
69	46±4	289±17	556±46	75±2.4 D (~5.75)

[a]Numbers in parentheses represent approximate Brinell hardness values.

The samples were prepared by casting a 5.0 wt % dimethylformamide solution on quartz plates. The solvent was evaporated by maintaining the plates at a temperature of 65 °C for three days. The thickness of the produced samples was several micrometers. Surface roughness measurements were obtained with an atomic force microscope (AFM) (Autoprobe MN5, Park Scientific Instruments). The root-mean-square (rms) surface roughness of all the samples (determined from 4 μm×4 μm surface area AFM images) was found to be less than 10 nm.

B. Scanning force microscopy

Nanomechanical testing was performed with a scanning force microscope consisting of an AFM (Nanoscope II, Digital Instruments) retrofitted with a capacitive force transducer (Triboscope, Hysitron, Inc.). The vertical and lateral forces in the indentation and friction experiments were determined from two independent capacitor plates that were previously calibrated following the procedure outlined in Refs. 15 and 16. A conical diamond tip with a nominal radius of curvature of ~20 μm was used in all the experiments. The tip was cleaned with isopropanol before each set of tests. In both the nanoindentation and the friction experiments, the normal load was varied in the range of 10–500 μN. In all tests, the tip was first engaged with the specimen surface under a contact force of 2 μN in order to set the reference point.

Nanoindentations were performed using a trapezoidal loading path with a constant load/unload rate equal to 50 μN/s. An experiment comprised indenting the specimen to a specified maximum load, maintaining the maximum load for 5 s (hold period), and then unloading the tip at the same rate as for the loading. Figure 4 shows a typical force versus displacement curve from an indentation experiment, illustrating the loading and unloading responses of the indented material and the pertinent nomenclature.

Friction testing involved traversing the diamond tip under a given load over the specimen surface at a speed of 4, 8, and 24 μm/min for a total distance of sliding equal to 4 μm. The coefficient of friction was obtained as the ratio of the average friction force to the applied normal force. The steady-state friction coefficient was calculated by averaging the friction data acquired between 1 and 3 μm of sliding distance.

The results presented later correspond to average values obtained from at least five experiments, assuming that the data followed normal distributions. A good reproducibility was obtained from sample to sample. The error bars in the following figures (corresponding to one standard deviation above and below the mean values) reflect the statistical scatter in the experiments. Mechanical testing was performed in a clean-air laboratory environment of temperature equal to ~25 °C and relative humidity between 40% and 50%.

C. Measurement of mechanical properties

Some of the quantities and analytical relations used in nanoindentation are described in this section for completeness. Because the displacements during unloading are elastic, the relation between the unloading curve and the elastic modulus of the indented material can be obtained from elasticity theory. The contact compliance C_e for an axisymmetric indenter and an isotropic elastic half-space is given by[17]

$$C_e = \frac{dh}{dP} = \frac{\sqrt{\pi}}{2\sqrt{A}E_r},$$

where h is the displacement of the indenter relative to the free surface of the specimen (indentation depth), P is the applied normal load, A is the corresponding projected contact area, and E_r is the reduced elastic modulus given by $E_r = [(1-\nu_s^2)/E_s + (1-\nu_i^2)/E_i]^{-1}$, where E and ν are the elastic modulus and Poisson's ratio, and subscripts s and i denote the sample and indenter materials, respectively. For polymer materials and diamond indenter, $E_i \gg E_s$, and, hence, it may be assumed that $E_r = E_s/(1-\nu_s^2)$. Because all the samples are elastomers, it was assumed that $\nu_s = 0.45$.

Since the determination of the tip shape function $A(h_c)$ is based on the measurement of the contact stiffness S (i.e., the reciprocal of the contact compliance), imaging of the indentation is not required.[18] The unloading curve can be described by a power-law function.[17] The slope of the tangent to the power-law curve at the maximum indentation load represents the material stiffness $S = dP/dh$ (Fig. 4). The contact area can be determined from the tip shape function $A(h_c)$, represented by a polynomial function of the form

$$A(h_c) = C_0 h_c^2 + C_1 h_c + C_2 h_c^{1/2} + C_3 h_c^{1/4} + C_4 h_c^{1/8} + C_5 h_c^{1/16} + \cdots$$

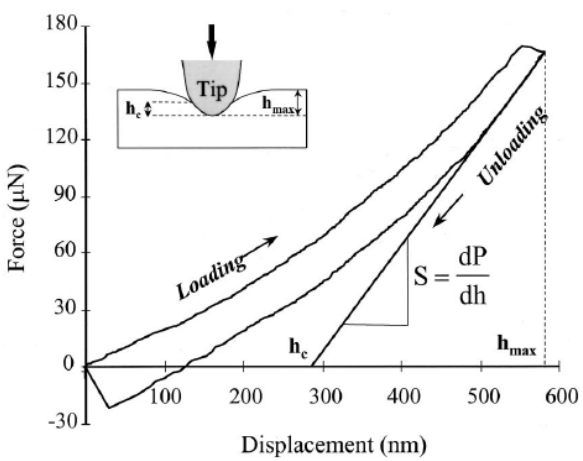

FIG. 4. Typical force vs displacement curve obtained from a nanoindentation experiment.

In this study, the area function was determined for the range of contact depths expected in the nanoindentation experiments (on the order of several hundreds of nanometers). An optically smooth polycarbonate (PC) sample, with an elastic modulus of 2.95 GPa and a Poisson's ratio of 0.38,[19] was used to calibrate the tip. From several indentations performed on the PC sample, the coefficients of the shape function were found to be $C_0=24.5$, $C_1=0.87\times10^5$, $C_2=-0.6\times10^6$, $C_3=0.37\times10^6$, $C_4=6.16\times10^6$, and $C_5=-5.83\times10^6$. Since the addition of more terms produced negligible changes in the shape function estimates, $A(h_c)$ was approximated by a six-term polynomial function. PC has been adopted as the standard material for tip calibration in nanoindentation studies of polymers due to the good repeatability of the experimental measurements, insignificant adhesion, and negligible loading rate effects.[16] The calibration curve was obtained by indenting the PC sample following the same loading and unloading procedures as in the indentation of the PUR samples using contact loads between 50 and 3000 μN.

In addition to the elastic modulus measurements, hardness values were extracted from the obtained nanoindentation curves (Fig. 4). Hardness is defined as $H=P_{\max}/A_{\max}$, where $P_{\max}$ is the maximum load applied during the indentation experiment and $A_{\max}$ is the corresponding projected contact area.[18] Traditionally, the elastic contribution to the indentation hardness is subtracted by measuring the projected area of the residual impression, i.e., the projected contact area is measured after the sample has recovered elastically.[20] However, it was impossible to clearly discern any topographical changes after indentation due to the profound elastic recovery of the PUR samples. Hence, the hardness measurements presented here were calculated using the projected contact area corresponding to the maximum indentation load, i.e., without accounting for viscoelastic material recovery effects.

III. RESULTS AND DISCUSSION

A. Surface mechanical properties

Results for the hardness and elastic modulus of the different PUR compositions determined from the nanoindentation material responses are interpreted in this section. Figure 5 shows typical nanoindentation curves of the softer PUR composition (42 wt % HS). The load-displacement curves follow fairly closely the same loading and unloading paths for different maximum contact loads, reflecting a good reproducibility of the results. An increase of the maximum displacement during the 5 s hold period, i.e., when the maximum load was maintained approximately constant by the load transducer, and an attractive (adhesive) force during unloading of the tip occurred in all the tests. This relaxation behavior of the material under nearly constant load has been used to evaluate the time-dependent deformation behavior of polymers at submicron scales.[16] It is noted that both the tendency of the material to relax and the magnitude of the adhesive force increase with the maximum indentation load. Qualitatively similar results were found for the other PUR compositions.

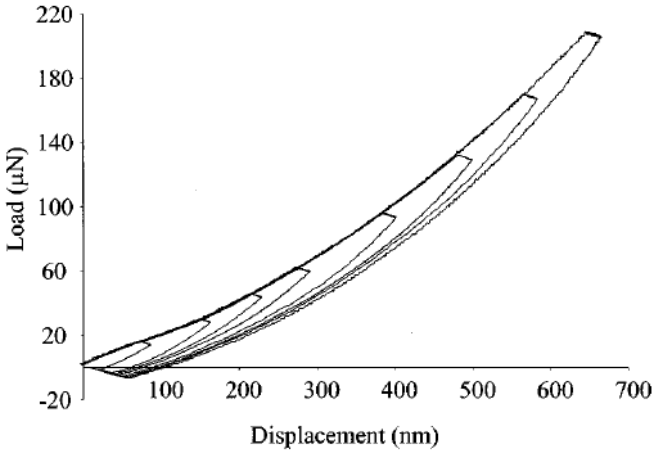

FIG. 5. Nanoindentation curves of PUR containing 42 wt % HS for different maximum contact loads.

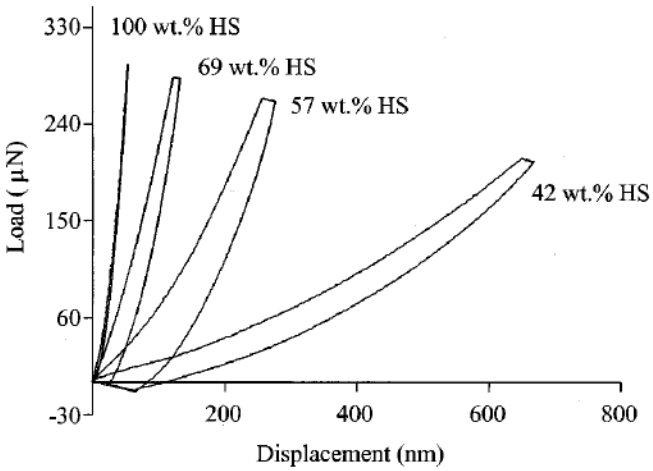

FIG. 6. Nanoindentation curves of PUR containing 42, 57, 69, and 100 wt % HS.

Figure 6 shows a comparison of representative indentation curves for the different PUR compositions. A remarkably different behavior was obtained by varying the HS content. For 100 wt % HS, the loading and unloading paths are essentially linear and almost overlapping, suggesting a nearly linear elastic behavior. However, a viscoelastic behavior revealing time-dependent deformation during the hold period at maximum load and a noticeable adhesion force upon unloading were encountered for lower HS contents, especially for 57 and 42 wt % HS. The profound change in the slope of the unloading curve and the increase of the maximum penetration depth suggest that both the material stiffness and the indentation hardness decreased with decreasing HS content. This behavior may be attributed to the effect of microphase separation on the mechanical properties, which becomes more pronounced at higher HS contents.

Figure 7 shows the material hardness as a function of contact depth. While for 42 wt % HS the hardness is nearly constant, for higher HS contents it increases remarkably with the contact depth (or indentation load). A similar trend has been reported for the indentation hardness of low- and high-density polyethylene and different grades of ultrahigh molecular weight polyethylene.[16] This dependence of the PUR hardness on contact depth can be explained by considering the effect of contact pressure on the mobility of macromolecules. When the diamond tip compresses the polymer sample, the free volume of the macromolecules decreases.

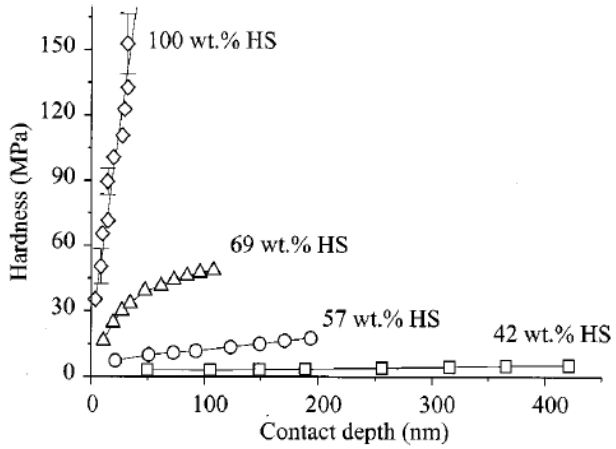

FIG. 7. Hardness vs contact depth of PUR containing 42, 57, 69, and 100 wt % HS. (Error bars not shown are smaller than the symbol size.)

This increases the resistance to deformation and the polymer behaves as a harder material. This effect becomes more pronounced at higher contact pressures (i.e., deeper indentations) and higher HS contents because the HS are less compressible than the SS. In addition, since the density of the HS crystalline phase is higher than that of the amorphous SS phase,[21] the average density increases with the HS content, which is beneficial to the penetration resistance of the polymer.

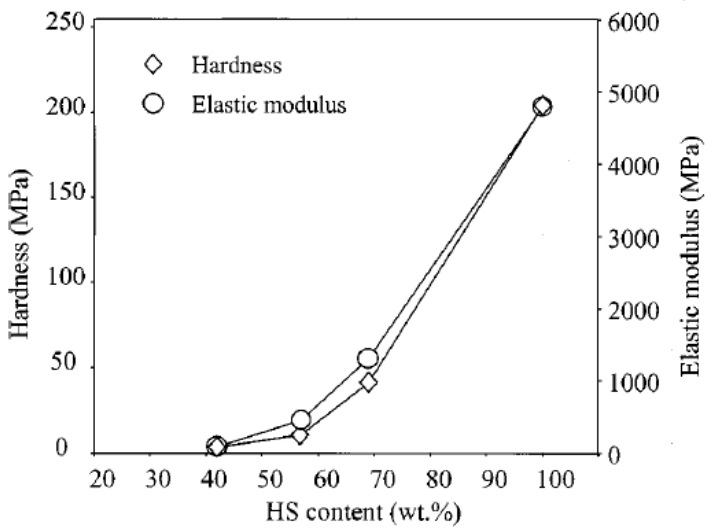

FIG. 8. Hardness and elastic modulus of PUR vs HS content.

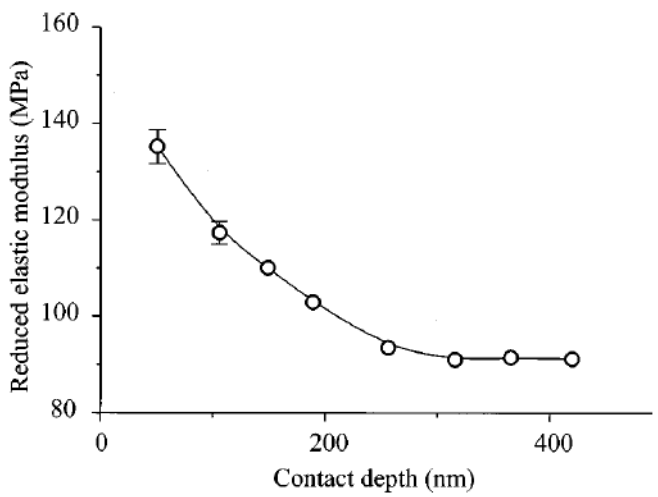

FIG. 9. Reduced elastic modulus vs contact depth of PUR containing 42 wt % HS. (Error bars not shown are smaller than the symbol size.)

Figure 8 shows that both the hardness and the elastic modulus of PUR increase with the HS content. The hardness values correspond to a maximum indentation depth of ~50 nm. The elastic modulus values were determined for a maximum indentation load greater than 200 μN. The nonlinear increase of the hardness and the elastic modulus with the HS content may be attributed to the higher concentration of crystalline microdomains at higher HS contents. The results shown in Fig. 8 provide additional evidence about the enhancement of the mechanical properties of PUR by microphase separation. This trend for the elastic modulus is in qualitative agreement with measurements obtained from standard tensile tests (Table II). However, the elastic modulus values obtained from the nanoindentation experiments are much higher than typical bulk values quoted from the literature. This discrepancy can be explained by considering the dependence of the material behavior on the type and rate of loading during mechanical testing. As mentioned previously, in the indentation tests the material is under compression and the mobility of the macromolecules under the tip is constrained, whereas in the tensile tests the macromolecules are relatively less constrained. Thus, a different material response is encountered in each type of experiment. In addition, since the loading rate in the nanoindentation experiments is significantly higher than that in conventional pull tests, the polymer may exhibit an increased resistance to deformation due to the insufficient time for macromolecule movement and relaxation.

Figure 9 shows the reduced elastic modulus, equal to $E_s/(1-\nu_s^2)$, as a function of contact depth for the sample containing 42 wt % HS. The elastic modulus decreases with increasing maximum contact load (or contact depth) reaching a constant value at a depth of ~300 nm. The elastic modulus is normally expected to be constant and independent of indentation depth.[17] However, strain hardening may affect the material behavior underneath the indenter. Indented materials exhibiting mild strain hardening yield pileups at the boundaries of the contact region. It was found that the indented PUR with the lowest HS content demonstrated marginal strain hardening. Since this PUR can be easily deformed, pileup formation should have been more pronounced for this material. The projected contact area determined from the tip calibration performed on a PC sample may differ from those obtained with elastomers. Since the elastic modulus of PC is much greater than that of PUR elastomers, PC does not exhibit a pileup effect and the deformation under the tip is predominantly plastic. As a consequence, the contact area in the experiments with the softer PUR might have been underestimated. Thus, in view of the proportionality dependence of the reduced elastic modulus on the reciprocal of the square root of the projected contact area, the elastic modulus values might have been overestimated. However, the pileup effect is negligibly small at high contact loads (or large contact depths) because the resulting contact area is significantly larger than the pileup regions.

Although the trend observed with the other PUR compositions was similar to that shown in Fig. 9, the variation of the elastic modulus with contact depth was less pronounced. For the 57 and 69 wt % HS contents, the elastic modulus did not show any variation at depths greater than 50 and 20 nm, respectively. This may be attributed to the reduced pileup

effect on the deformation of the stiffer and harder PUR compositions. For 100 wt % HS, the elastic modulus increased slightly with contact depth reaching a maximum at a depth of ~30 nm. Similar results have been observed in other studies,[22] and have been attributed to the increase of the density of the polymer (due to the interaction of polymer chains) which enhances the elastic modulus,[23] and changes of the relaxation behavior of the polymer chains that also contribute to the increase of the polymer stiffness.[24] Nevertheless, the possible underestimation of the projected contact area at light indentation loads due to the pileup effect was not a factor in the determination of the elastic modulus data plotted in Fig. 8 because the maximum indentation load in these experiments was greater than 200 μN.

B. Friction characteristics

Figure 10 shows representative coefficient of friction results for different HS contents, contact load equal to 100 μN, and sliding speed fixed at 8 μm/min. It is noted that the friction behavior of PUR depends strongly on the HS content. For 42 and 57 wt % HS, the coefficient of friction increased rapidly reaching a peak value μ_{max}. At that juncture, the high friction torque caused the tip to tilt. When the strain energy in the system exceeded the work of adhesion at the tip/sample interface, the tip began to slide over the polymer surface producing a steady-state friction coefficient μ_{ss} less than μ_{max}. Although a rapid decrease in the coefficient of friction from a peak value did not occur for 69 wt % HS, a higher friction coefficient was obtained at steady state. The average values of μ_{ss} in Fig. 10 corresponding to 42, 57, and 69 wt % HS contents are equal to 0.6, 0.4, and 0.9, respectively.

Depending on the polymer composition, different trends for the tip normal displacement were encountered during friction testing. During sliding, the tip sunk into the PUR sample with 42 wt % HS, and the penetration depth increased from ~265 nm at the onset of sliding to ~400 nm at the end of the test. However, in the sliding experiments with the PUR containing 57 wt % HS, the penetration depth decreased only slightly, whereas for the 69 wt % HS content the depth decreased gradually. The penetration depth measured at the onset of sliding ($x=0$) and at the end of sliding ($x=4$ μm) is given in Table III along with the steady-state coefficient of friction and the calculated deviation angle indicating the slope of the sliding path of the tip. Several friction tests confirmed the reproducibility of these sliding patterns of the tip for each PUR composition.

The previous observations for the polymer deformation behavior during sliding may be associated with composition differences. In the experiments with the softer PUR, the contact depth increased in order to compensate for the relaxation of the material under the normal and shear traction. Since material relaxation was less pronounced in the sample with 57 wt % HS, the contact area did not increase to support the load and, thus, the tip slid on the sample surface plowing through the material at nearly constant depth. Consequently, the produced smaller contact area resulted in a lower friction coefficient [Fig. 10(b)]. However, in the case of the harder sample (69 wt % HS), ridge formation occurred at the front

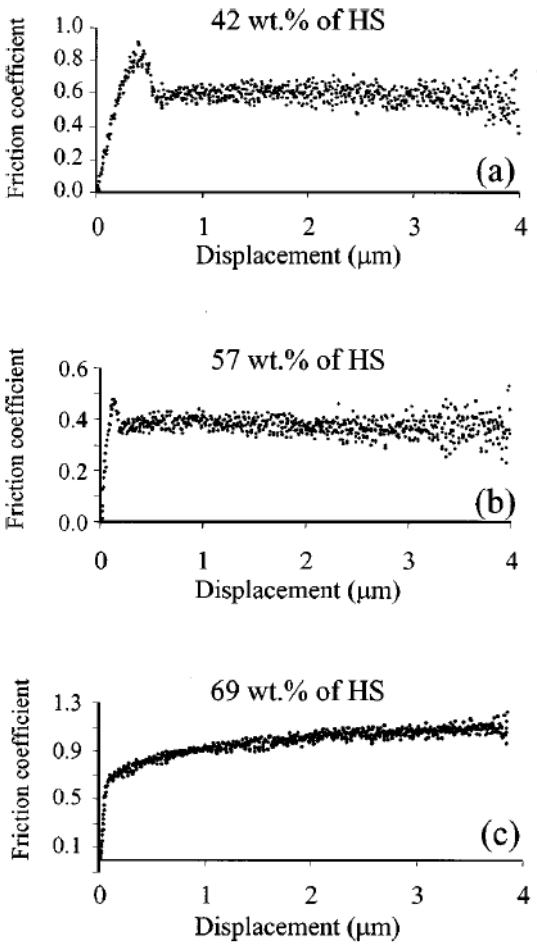

FIG. 10. Coefficient of friction vs sliding distance of PUR for 100 μN contact load, 8 μm/min sliding speed, and HS content equal to (a) 42, (b) 57, and (c) 69 wt %.

of the tip. Thus, contrary to the softer sample, the tip had to retract in order to climb over the ridge, and while this reduced the penetration depth, it increased the coefficient of friction [Fig. 10(c)].

Figure 11 shows the dependence of the friction coefficient of different PUR compositions on contact load and sliding speed. Considering the experimental uncertainty in the data, it may be argued that both the load and the sliding speed exhibited a very small effect on the friction behavior of the PUR with 57 wt % HS. The average value of the friction coefficient for loads equal to 10, 100, and 500 μN and sliding speeds of 4, 8, and 24 μm/min is equal to 0.33 $\pm$0.08, which is of the same order of magnitude with the kinetic friction coefficient values reported for metals sliding against polyurethanes.[25,26] This relatively low friction coefficient suggests that polymer material did not adhere to the diamond tip during sliding.

The general trend in Fig. 11 is for the friction coefficient to decrease with increasing contact load and sliding speed. This may be attributed to the effect of surface roughness. At high contact loads, the roughness effect on the friction behavior is secondary because the tip plows through the material. Alternatively, at light contact loads the tip follows the surface topography and the roughness effect on the friction force is significant. The decrease of the friction coefficient with increasing sliding speed can be explained in terms of the dwell time of the tip and the relaxation rate of the polymer. At high sliding speeds, the high shear strain rates induced by the tip occurred within a very short time period for time-dependent deformation (relaxation) to take place. Since

the contact area is affected by the relaxation process, which is controlled by the polymer microstructure, the smaller contact areas produced at high sliding speeds under the same load yielded lower friction coefficients. In addition, frictional heating at high sliding speeds might have affected the magnitude of the friction force by enhancing the relaxation rate of the material.

The variability in the friction characteristics of the different PUR compositions observed in this study can be attributed to the extent of microphase separation in the bulk material. The microdomains produced from phase separation possess higher cohesion and greater resistance to deformation during sliding. It is clear, therefore, that microphase separation contributed significantly to the friction behavior of PUR. In addition, the molecular weight affects the shear resistance of the plowed polymer surfaces. The entanglement of macromolecules increases with the molecular weight, resulting in three-dimensional networks resisting alignment parallel to the direction of sliding. Hence, in view of the microphase separation and molecular weight effects on the mechanical behavior of PUR elastomers and the results shown in Figs. 10 and 11, the friction coefficient can be considered as a function of both intrinsic material properties of the PUR, such as HS content and M_w, and extrinsic properties, such as contact load and sliding speed (shear rate).

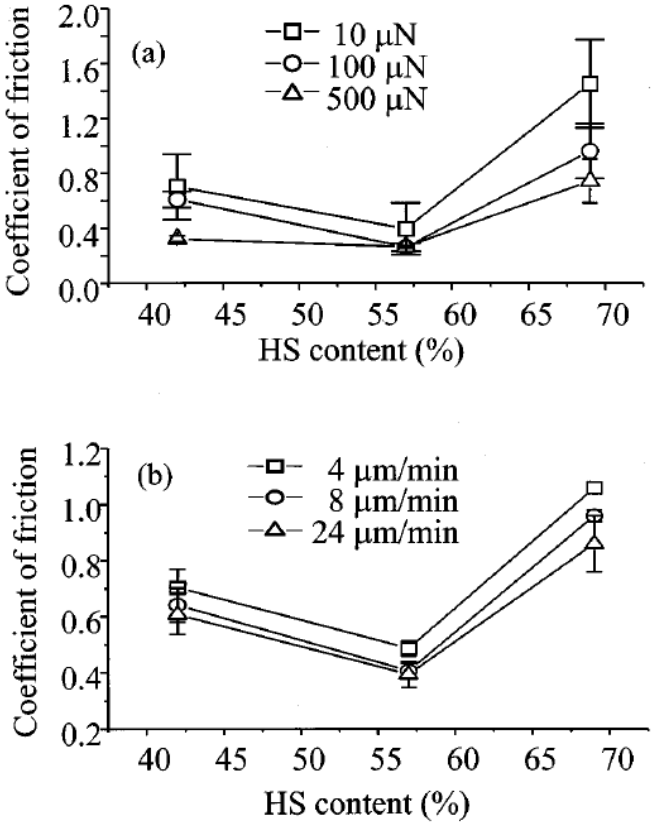

FIG. 11. Coefficient of friction vs HS content of PUR for (a) contact load equal to 10, 100, and 500 μN and sliding speed of 8 μm/min, and (b) contact load equal to 100 μN and sliding speed of 4, 8, and 24 μm/min.

TABLE III. Normal displacement of indenter tip during friction testing.

HS (wt %)	Steady-state friction coefficient μ_{ss}	Normal displacement ($x=0$ μm) (nm)	Normal displacement ($x=4$ μm) (nm)	Deviation angle (deg.)
42	0.6	−265±2	−396±3	−1.9
57	0.4	−105±1	−131±5	−0.4
69	0.9	−69±1	0.4±3	+1.0

IV. CONCLUSIONS

The mechanical and friction properties of PUR with different HS contents were evaluated in light of nanoindentation and friction experiments performed with a surface force microscope. Based on the presented results and discussion, the following main conclusions can be drawn.

(1) Deformation is controlled by the extent of microphase separation, which involves hydrogen-bonded and nonbonded HS. Urethane groups associated with each other through hydrogen bonding result in the formation of small crystalline domains.

(2) The hardness increases with the indentation load (or contact depth). A decrease of the elastic modulus with increasing contact depth was observed for the softer PUR (42 wt % HS) and was attributed to pileup formation at the boundaries of the contact region, which influenced the measurement of the projected contact area.

(3) The evaluation of the mechanical properties at the submicrometer scale confirmed that microphase separation, which is controlled by the HS content, greatly affects the hardness and elastic modulus of PUR elastomers.

(4) Different friction behaviors were observed, depending on the composition of the samples. The lowest and highest steady-state friction coefficients were found for 57 and 69 wt % HS, respectively. The remarkable differences in the friction characteristics were related to variations in the polymer composition affecting the deformation behavior.

(5) The decrease of the friction coefficient with increasing contact load and sliding speed was attributed to surface roughness effects and the relaxation of the polymer materials.

(6) The mechanical properties of PUR elastomers depend on the concentration of hydrogen bonds, which increases with the HS content yielding a higher cohesive strength. The relaxation process depends on the HS content and is affected by hydrogen bonding and microphase separation.

ACKNOWLEDGMENTS

This research was partially supported by the National Science Foundation under Grant No. CMS-0085156, and the University of California at Berkeley through a 1999–2001 Research Bridging Grant. The financial support provided to the first author by CNRS (France) and a NATO grant is also gratefully acknowledged.

Bibliography

[1] S. L. Cooper and A. V. Tobolsky, J. Appl. Polym. Sci. **10**, 1837 (1966).
[2] D. S. Huh and S. L. Cooper, Polym. Eng. Sci. **11**, 369 (1971).
[3] S. L. Samuels and G. L. Wilkes, J. Polym. Sci.: Symp. **43**, 149 (1973).
[4] Z. Wirpsza, in *Polyurethanes, Chemistry, Technology and Applications*, Polymer Science and Technology Series, GB, edited by E. Horwood (1993).
[5] T. Tanaka, T. Yokoyama, and Y. Yamaguchi, J. Polym. Sci., Part A-1 **6**, 2153 (1969).
[6] K. Nakamae, T. Nishino, S. Asaoka, and Sudaryanto, Int. J. Adhesion and Adhesives **16**, 233 (1996).
[7] R. W. Seymour and S. L. Cooper, Polym. Lett. **9**, 689 (1971).
[8] C. G. Seefried, J. V. Koleske, and F. E. Critchfield, J. Appl. Polym. Sci. **19**, 2493 (1975).
[9] I. D. Fridman and E. L. Thomas, Polymer **21**, 388 (1980).
[10] J. A. Miller, S. L. Cooper, C. C. Han, and G. Pruckmayr, Macromolecules **17**, 1063 (1984).
[11] J. T. Koberstein and T. P. Russell, Macromolecules **19**, 714 (1986).
[12] C. D. Eisenbach, A. Ribbe, and C. Günter, Macromol. Rapid Commun. **15**, 395 (1994).
[13] D. J. Martin, G. F. Meijs, G. M. Renwick, P. A. Gunatillake, and S. J. McCarthy, J. Appl. Polym. Sci. **60**, 557 (1996).
[14] J. Blackwell and C. D. Lee, J. Polym. Sci.: Polym. Phys. Ed. **21**, 2169 (1983).
[15] W. Lu and K. Komvopoulos, J. Appl. Phys. **85**, 2642 (1999).
[16] C. Klapperich, K. Komvopoulos, and L. Pruitt, J. Tribol. **123** (to appear, 2001).
[17] G. M. Pharr, W. C. Oliver, and F. R. Brotzen, J. Mater. Res. **7**, 613 (1992).
[18] K. W. McElhaney, J. J. Vlassak, and W. D. Nix, J. Mater. Res. **13**, 1300 (1998).
[19] L. Pruitt and D. Rondinone, Polym. Eng. Sci. **36**, 1300 (1996).
[20] N. A. Burnham and R. J. Colton, J. Vac. Sci. Technol. A **7**, 2906 (1989).
[21] J. T. Koberstein and L. M. Leung, Macromolecules **25**, 6205 (1992).
[22] D. H. Gracias and G. A. Somorjai, Macromolecules **31**, 1269 (1998).
[23] J. Sayre, S. Swanson, and R. Boyd, J. Polym. Sci.: Polym. Phys. Ed. **16**, 1739 (1978).
[24] S. V. Radcliffe, in *Deformation and Fracture of Polymers*, edited by H. H. Kausch, J. A. Hassell, and R. I. Jaffe (Plenum, New York, 1973), p. 198.
[25] *Handbook of Chemistry and Physics*, 76th ed. (CRC Press, Boca Raton, FL, 1996).
[26] *Polymer Handbook*, edited by J. Brandrup, E. H. Immergut, E. A. Grulke, A. Abe, and D. R. Bloch, 4th ed. (Wiley, New York, 1999).